

Extension of the discrete sources method to light scattering by highly elongated finite cylinders

ELENA EREMINA[†], YURI EREMIN[‡] and
THOMAS WRIEDT[†]

[†]Institut für Werkstofftechnik, Badgasteiner Strasse 3, 28359
Bremen, Germany

[‡]Moscow State University, Lenin's Hills, 119992 Moscow, Russia
e-mails: eremina@iwt.uni-bremen.de; thw@iwt.uni-bremen.de

(Received 19 February 2003; revision received 30 June 2003)

Abstract. Light scattering by long finite cylinders is applied for particle characterization, investigation of scattering and absorption properties of interstellar dust, ice crystals and many other fields. In recent years many methods have been used to solve this problem, but usually their applicability is restricted to aspect ratios of about 10. In this paper a renewed algorithm of the discrete sources method is described, which allows computer simulation of light scattering by highly elongated cylinders with aspect ratios up to 100 and length up to 40 μm .

1. Introduction

During recent years, many computational models have been developed to study light scattering by elongated particles. As a rule axially symmetric models are involved in the investigation of such particles. Various methods usually applied to solve this problem cannot be employed for investigating particles with aspect ratio more than 10. As far as we know the standard **T**-matrix method fails for particles having an aspect ratio of more than 5. Another method developed to simulate scattering by prolate spheroids is based on the field expansion in spheroidal wave functions. Scattering by particles with an aspect ratio of 2 has been demonstrated using this method [1]. In this context the generalized multipole technique (GMT) [2] looks very attractive. Results for a cylinder with an aspect ratio of 3 have been presented by Al-Rizzo and Tranquilla [3]. Using another variant of GMT [4], results for cylinders have also been published by our group [5]. In the context of the null-field method with discrete sources (NFM-DS) an aspect ratio of 20 has been achieved for spheroids [6]. In this paper we focus on the development of the discrete sources method (DSM). A new modified scheme of DSM allows us to analyse scattering by very elongated particles with a high refractive index. This new scheme enables us to obtain more accurate simulation results, to provide a monotonic decrease in the surface residual and to reduce the demand for computer resources compared with the conventional DSM model. Also it allows us to extend the range of validity of the DSM to particles of larger diameter. A similar approach has recently been applied to evanescent wave scattering [7]. Section 1 of the paper is a short review of the problem and methods for solving it. In section 2 of the paper we present the mathematical statement of the scattering problem and some

necessary theoretical results as well. The conventional DSM scheme is also presented in section 2 of the paper. Section 3 of the paper contains a detailed description of the numerical DSM scheme and focuses on the difference between the new approach and the conventional approach [8]. All the representations for matrix elements and far-field patterns are also given. Section 4 presents a detailed analysis of numerical results obtained via a FORTRAN programme based on the new approach.

2. Mathematical model

Let us start with the mathematical statement of the scattering problem. We consider scattering in an isotropic homogeneous medium in R^3 of an electromagnetic wave by a local homogeneous penetrable obstacle D_i with the smooth boundary ∂D . The geometry of scattering problem in a plane of scattering $\varphi = 0$ is depicted in figure 1, where \mathbf{k} shows the direction of the incident wave, z is an axis of a cylindrical coordinate system (z, θ, φ) , and θ_0 is the incident angle of a plane wave.

We assume the time dependence to be $\exp(j\omega t)$. Scattering is described by the electromagnetic fields $\{\mathbf{E}_\xi, \mathbf{H}_\xi\}$ satisfying the Maxwell equations

$$\begin{aligned} \nabla \times \mathbf{H}_\xi &= jk\varepsilon_\xi \mathbf{E}_\xi \\ \nabla \times \mathbf{E}_\xi &= -jk\mu_\xi \mathbf{H}_\xi \quad \text{in } D_\xi, \quad \xi = e, i, \quad D_e := \frac{R^3}{D_i}, \end{aligned} \tag{1}$$

the boundary conditions enforced on the particle surface given by

$$\begin{aligned} \mathbf{n}_p \times [\mathbf{E}_i(P) - \mathbf{E}_e(P)] &= \mathbf{n}_p \times \mathbf{E}^0(P) \\ \mathbf{n}_p \times [\mathbf{H}_i(P) - \mathbf{H}_e(P)] &= \mathbf{n}_p \times \mathbf{H}^0(P) \end{aligned} \quad P \in \partial D, \tag{2}$$

and the Silver-Muller radiation condition at infinity given by

$$\lim_{r \rightarrow \infty} \left(\varepsilon_e^{1/2} \mathbf{E}_e \times \frac{\mathbf{r}}{r} - \mu_e^{1/2} \mathbf{H}_e \right) = 0, \quad r = |M| \rightarrow \infty. \tag{3}$$

Here $\{\mathbf{E}^0, \mathbf{H}^0\}$ is an exciting field, \mathbf{n}_p is the unit outward normal to ∂D , \times is the sign for a vector product, the subscript e indicates the external domain D_e , the subscript

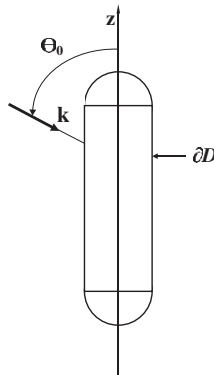


Figure 1. Model geometry.

i indicates the domain inside the particle D_i , ε_ξ is the permittivity, μ_ξ is the permeability, $\text{Im } \varepsilon_e, \text{Im } \mu_e = 0, \text{Im } \varepsilon_i \leq 0$ and $\text{Im } \mu_i \leq 0$. The boundary value scattering problem is well known to have a unique solution [9].

In the framework of the DSM the approximate solution is constructed as a finite linear combination of the field of dipoles and multipoles deposited in a supplementary domain. Under these conditions the representation satisfies Maxwell equations in D_i and D_e and radiation conditions at infinity. The unknown amplitudes of discrete sources (DSs) are to be determined from the boundary conditions at ∂D . So, the boundary value scattering problem under investigation reduces to the solution of the approximation problem enforced at the obstacle surface [8].

One of the most attractive features of the DSM is a flexible choice of DS fields that can be used for approximate solution construction. Additionally there are no limitations to a choice of support of DS, which should provide fulfilling Maxwell equations, radiation conditions and yield a complete system of DS fields at the obstacle surface [8].

We shall consider an axial symmetrical particle; then the system of lowest order multipoles distributed over the axis of symmetry can be applied to construct an approximation solution. As a consequence the surface approximating problem can be reduced to a number of one-dimensional problems enforced at the particle generatrix.

Let the axis of symmetry be the z axis, and DS $\{z_n\}_{n=1}^\infty$ be distributed over a segment ω_0 of the z axis, situated inside the particle, which is chosen as a closed multitude with at least one condensing point. Then the follow results are valid [10]:

- (i) Let the DS support be ω_0 ; then the associated system of electrical lowest-order distributed multipoles

$$\begin{aligned} \nabla \times \nabla \times [Y_m^e(\eta, z_n^e)\{1, \cos(m\varphi), \sin(m\varphi)\}\{\mathbf{e}_i\}], \\ \eta \in L, \{z_n^e\} \in \omega_0, \quad n, m \in N, \end{aligned} \tag{4}$$

where L , the generatrix of ∂D , is a complete system at any closed smooth axial symmetric surface, confining ω_0 . Here $Y_m^e(\eta, z_n^e) = h_m^{(2)}(k_e R_{\eta z_n^e})(r/R_{\eta z_n^e})^m$, where $h_m^{(2)}(\cdot)$ is the spherical Hankel function, $R_{\eta z_n} = r^2 + (z - z_n)^2$, z_n^e are multipole coordinates inside the particle and $\{\mathbf{e}_i\} = \{e_x, e_y, e_z\}$ is a vector basis in the Cartesian coordinate system.

- (ii) The system of magnetic multipoles distributed over ω_0 is complete

$$\nabla \times [Y_m^e(\eta, z_n^e)\{1, \cos(m\varphi), \sin(m\varphi)\}\{\mathbf{e}_i\}], \quad n, m \in N. \tag{5}$$

- (iii) For the internal fields representation, similar results hold. The system of electrical lowest-order regular functions is complete at ∂D_i

$$\nabla \times \nabla \times [Y_m^i(\eta, z_n)\{1, \cos(m\varphi), \sin(m\varphi)\}\{\mathbf{e}_i\}], \quad n, m \in N, \tag{6}$$

where $Y_m^i(\eta, z_n) = j_m(k_i R_{\eta z_n})(r/R_{\eta z_n})^m$, $j_m(\cdot)$ is the spherical Bessel function. The same result may be formulated for the system of magnetic regular functions:

$$\nabla \times [Y_m^i(\eta, z_n)\{1, \cos(m\varphi), \sin(m\varphi)\}\{\mathbf{e}_i\}]. \tag{7}$$

These systems represent systems of regular functions, which satisfy Maxwell equations in the whole space R^3 .

We shall construct the approximate solution by taking into account not only the rotational symmetry of the obstacle but also the polarization of an external excitation as well.

In the case of a p-polarized exciting plane wave the exciting field accepts the following form:

$$\begin{aligned} \mathbf{E}^0 &= (\mathbf{e}_x \cos \theta_0 + \mathbf{e}_z \sin \theta_0)\gamma, \\ \mathbf{H}^0 &= -\mathbf{e}_y \gamma \cos \theta_0, \\ \gamma &= \exp[-jk_e(x \sin \theta_0 - z \cos \theta_0)], \end{aligned} \tag{8}$$

where $k_e = k(\epsilon_e \mu_e)^{1/2}$.

To take the polarization of the external excitation into account we use some linear combination of electrical and magnetic multipoles. For this we need special vector potentials. In the case of p polarization of the plane wave the representation for vector potentials in a cylindrical coordinate system can be represented as

$$\begin{aligned} \mathbf{A}_{mn}^{1,e,i} &= \{Y_m^{e,i}(\rho, z_n^{e,i}) \cos[(m+1)\varphi]; -Y_m^{e,i}(\rho, z_n^{e,i}) \sin[(m+1)\varphi]; 0\}, \\ \mathbf{A}_{mn}^{2,e,i} &= \{Y_m^{e,i}(\rho, z_n^{e,i}) \sin[(m+1)\varphi]; Y_m^{e,i}(\rho, z_n^{e,i}) \cos[(m+1)\varphi]; 0\}. \end{aligned} \tag{9}$$

Vector potentials for vertical dipoles, which are required to be added to provide completeness of the multipoles' system are

$$\mathbf{A}_n^{3,e,i} = \{0, 0, Y_0^{e,i}(\rho, z_n^{e,i})\}. \tag{10}$$

So, the approximate solution taking into account p polarization of the plane wave, axial symmetry of the particle, can be represented in the form

$$\begin{pmatrix} \mathbf{E}_\xi^N \\ \mathbf{H}_\xi^N \end{pmatrix} = \sum_{m=0}^M \sum_{n=1}^{N_\xi^m} \{p_{mn}^\xi \mathbf{D}_1 \times \mathbf{A}_{mn}^{1,\xi} + q_{mn}^\xi \mathbf{D}_2 \times \mathbf{A}_{mn}^{2,\xi}\} + \sum_{n=1}^{N_\xi^0} r_n^\xi \mathbf{D}_1 \times \mathbf{A}_n^{1,\xi}, \tag{11}$$

were

$$\mathbf{D}_1 = \begin{pmatrix} \frac{j}{k\epsilon_\xi \mu_\xi} \nabla \times \nabla \\ -\frac{1}{\mu_\xi} \nabla \end{pmatrix}, \mathbf{D}_2 = \begin{pmatrix} \frac{1}{\epsilon_\xi} \nabla \\ \frac{j}{k\epsilon_\xi \mu_\xi} \nabla \times \nabla \end{pmatrix}. \tag{12}$$

Then the following result holds: The approximate solution (11) converges to the exact solution for $\{M, N_\xi^m\}$ tending to infinity.

In the case of an s-polarized plane wave the exciting field has the form:

$$\begin{aligned} \mathbf{E}^0 &= \mathbf{e}_y \gamma \cos \theta_0, \\ \mathbf{H}^0 &= (\mathbf{e}_x \cos \theta_0 + \mathbf{e}_z \sin \theta_0)\gamma. \end{aligned} \tag{12}$$

The vector potentials corresponding to this case are

$$\begin{aligned} \mathbf{A}_{mn}^{1,e,i} &= \{Y_m^{e,i}(\rho, z_n^{e,i}) \sin(m+1)\varphi; Y_m^{e,i}(\rho, z_n^{e,i}) \cos(m+1)\varphi; 0\}, \\ \mathbf{A}_{mn}^{2,e,i} &= \{Y_m^{e,i}(\rho, z_n^{e,i}) \cos(m+1)\varphi; -Y_m^{e,i}(\rho, z_n^{e,i}) \sin(m+1)\varphi; 0\}. \end{aligned} \tag{13}$$

Hence the approximate solution can be represented as

$$\begin{pmatrix} \mathbf{E}_\xi^N \\ \mathbf{H}_\xi^N \end{pmatrix} = \sum_{m=0}^M \sum_{n=1}^{N_\xi^m} \{ p_{mn}^\xi \mathbf{D}_1 \times \mathbf{A}_{mn}^{1,\xi} + q_{mn}^\xi \mathbf{D}_2 \times \mathbf{A}_{mn}^{2,\xi} \} + \sum_{n=1}^{N_\xi^0} r_n^\xi \mathbf{D}_2 \times \mathbf{A}_{0n}^{1,\xi}. \quad (14)$$

The approximate solution (14) corresponding to the s-polarized case converges to the exact solution for $\{M, N_\xi^m\}$ tending to infinity.

3. Numerical algorithm

Let us recall that the approximate solutions for the cases of p polarization (equation (11)) and s polarization (equation (14)) satisfy Maxwell's equations (1) and radiating conditions (3) at infinity. As the DSs are situated on the symmetry axis of the particle, the approximate solution is a finite linear combination of Fourier harmonics with respect to the φ variable. So, first we resolve the plane wave excitation into a Fourier series with respect to the φ variable, using the following resolution for the plane wave:

$$\exp(-jk_e \rho \sin \theta_0 \cos \varphi) = \sum_{m=0}^{\infty} (2 - \delta_{0m}) (-j)^m J_m(k_e \rho \sin \theta_0) \cos(m\varphi), \quad (15)$$

where θ_0 is the incident angle of the plane wave.

The approximate solution satisfies all the conditions of the original scattering problem, except the boundary conditions. Therefore, the unknown vector of the amplitudes of the DSs given by

$$\mathbf{p}_m = \{ p_{mn}^{e,i}, q_{mn}^{e,i}, r_n^{e,i} \}_{n=1}^{N_{e,i}^m} \quad (16)$$

where $p_{mn}^{e,i}$, $q_{mn}^{e,i}$ and $r_n^{e,i}$ are the amplitudes of the electric, magnetic and vector dipoles respectively in the representations (11) and (14), has to be determined from the transmission conditions (2). Taking into account the dependence of the plane wave on the φ angle, we can reduce the surface approximation problem enforced at the particle surface to a sequence of one-dimensional problems at the particle generatrix L . To solve this problem we use the general matching-point technique [11]. First we choose matching points $\{\eta_l\}_{l=1}^L$ distributed homogeneously over L . Then, by matching the representation for the approximate solution and external excitation at the set of matching points and using the axial symmetry we pass from the surface approximation to the approximation for each Fourier harmonic. As a consequence the unknown vectors \mathbf{p}_m can be found as a pseudosolution of an over-determined system of linear equations

$$\mathbf{I}_m \mathbf{p}_m = \mathbf{q}_m, \quad m = 0, \dots, M. \quad (17)$$

Here \mathbf{I}_m is a rectangular matrix of tangential components of multipole's fields [10], $\mathbf{I}_m = [B_{li}^m]$, $l = 1, \dots, 4L$, $i = 1, \dots, 2(N_1^m + N_e^m)$. The reasonable ratio of matching points and number of DSs was established as $2 < L/(N_1^m + N_e^m) < 4$; the vector \mathbf{p}_m of unknown amplitudes has the length $2(N_1^m + N_e^m)$ the vector on the right-hand side can be represented as a $4L$ vector, in the following form;

$$\mathbf{q}_m = \left(e_{m+1,l}^{0\tau}, e_{m+1,l}^{0\varphi}, h_{m+1,l}^{0\tau}, h_{m+1,l}^{0\varphi} \right)^T, \quad (18)$$

where $e_{ml}^{0\tau,\varphi} = e_{ml}^{0\tau,\varphi}(\eta_l)$, $h_{ml}^{0\tau,\varphi} = h_{ml}^{0\tau,\varphi}(\eta_l)$. The components of the vector, in the case of p-polarized plane wave excitation can be written as

$$\begin{aligned} e_{m+1}^{0\tau}(\eta) &= (-j)^m \alpha \cos \theta_0 \{ [J_m(k_e \rho \sin \theta_0) - J_{m+2}(k_e \rho \sin \theta_0)] \\ &\quad + 2j\beta \sin \theta_0 J_{m+1}(k_e \rho \sin \theta_0) \} \exp\{-jk_e z \cos \theta_0\}, \\ e_{m+1}^{0\varphi}(\eta) &= -\cos \theta_0 (-j)^m [J_m(k_e \rho \sin \theta_0) + J_{m+2}(k_e \rho \sin \theta_0)] \exp(-jk_e z \cos \theta_0), \\ e_{m+1}^{0\tau cs}(\eta) &= -\alpha (-j)^m [J_m(k_e \rho \sin \theta_0) + J_{m+2}(k_e \rho \sin \theta_0)] \exp(-jk_e z \cos \theta_0), \\ h_{m+1}^{0\varphi}(\eta) &= (-j)^m [-J_m(k_e \rho \sin \theta_0) + J_{m+2}(k_e \rho \sin \theta_0)] \exp(-jk_e z \cos \theta_0) \end{aligned} \quad (19)$$

In the case of s-polarized exciting wave,

$$\begin{aligned} e_{m+1}^{0\tau}(\eta) &= (-j)^m \alpha [J_m(k_e \rho \sin \theta_0) + J_{m+2}(k_e \rho \sin \theta_0)] \exp(-jk_e z \cos \theta_0), \\ e_{m+1}^{0\varphi}(\eta) &= (-j)^m [J_m(k_e \rho \sin \theta_0) - J_{m+2}(k_e \rho \sin \theta_0)] \exp(-jk_e z \cos \theta_0), \\ h_{m+1}^{0\tau}(\eta) &= (-j)^m [\alpha \cos \theta_0 (J_m(k_e \rho \sin \theta_0) - J_{m+2}(k_e \rho \sin \theta_0)) \\ &\quad + 2j\beta \sin \theta_0 J_{m+1}(k_e \rho \sin \theta_0)] \exp(-jk_e z \cos \theta_0), \\ h_{m+1}^{0\varphi}(\eta) &= -\cos \theta_0 (-j)^m [J_m(k_e \rho \sin \theta_0) + J_{m+2}(k_e \rho \sin \theta_0)] \exp(-jk_e z \cos \theta_0), \end{aligned} \quad (20)$$

where $(\alpha, 0, \beta)$ is a vector, tangential to the generatrix at the η point, and (ρ, z) correspond to the coordinates of the matching point.

Because Fourier harmonics do not depend on the φ angle, corresponding to vertical electric or magnetic dipoles the linear system for p and s polarization can be written in the form

$$\mathbf{l}_{-1} \mathbf{p}_{-1} = \mathbf{q}_{-1}.$$

In this case, \mathbf{l}_{-1} has the dimension $2L \times (N_i^m + N_e^m)$, the right-hand side vector has the length $2L$, and the unknown vector \mathbf{p}_{-1} of amplitudes has the length $N_i^m + N_e^m$. Then we have

$$\begin{aligned} e_0^{0\varphi}(\eta) &= -[j\alpha \cos \theta_0 J_1(k_e \rho \sin \theta_0) + \beta \sin \theta_0 J_0(k_e \rho \sin \theta_0)] \exp(-jk_e z \cos \theta_0), \\ h_0^{0\tau}(\eta) &= jJ_1(k_e \rho \sin \theta_0) \exp(-jk_e z \cos \theta_0), \end{aligned} \quad (21)$$

for p polarization and

$$\begin{aligned} e_0^{0\tau}(\eta) &= jJ_1(k_e \rho \sin \theta_0) \exp(-jk_e z \cos \theta_0) \\ h_0^{0\varphi}(\eta) &= -[j\alpha \cos \theta_0 J_1(k_e \rho \sin \theta_0) + \beta \sin \theta_0 J_0(k_e \rho \sin \theta_0)] \exp(-jk_e z \cos \theta_0) \end{aligned} \quad (22)$$

for s polarization. The main differences of the extended DSM scheme described above from the conventional DSM scheme [8] consist of the following.

- (i) Different numbers N_e^m and N_i^m of DS are used for the representation of the scattered field outside and total field inside the particle respectively. The numbers of DSs are chosen proportionally to the value of refractive index of the corresponding media. For the internal domain (higher refractive index $(\varepsilon_i \mu_i)^{1/2} > (\varepsilon_e \mu_e)^{1/2}$ we use a higher number of DSs than for the scattered field ($N_i^m > N_e^m$).
- (ii) The number of DSs depends on the rank of Fourier harmonics $N_\xi^m = N_\xi(m)$. For higher harmonics we use a lower number of multipoles ($N_\xi^{m+1} \leq N_\xi^m$). This circumstance enables us to acquire a more accurate simulation result, provides a monotonic decrease on the surface residual

and reduces the demand on computer resources up to 30% for a larger particles compared with the conventional DSM model. Also it allows us to extend the range of validity of the DSM to particles of larger diameters.

After DS amplitudes $\{\mathbf{p}_m\}_{m=1}^M$ have been determined, the far-field pattern can be computed [9]:

$$\frac{\mathbf{E}(\mathbf{r})}{|\mathbf{E}^0(\mathbf{r})|} = \frac{\exp(-jk_e r)}{r} \mathbf{F}(\theta, \varphi) + o\left(\frac{1}{r}\right), \quad r \rightarrow \infty. \quad (23)$$

The vector $\mathbf{F}(\theta, \varphi)$ has two components φ and θ in the far zone so that its components are determined at the unit sphere as

$$\mathbf{F}(\theta, \varphi) = \theta F_\theta(\theta, \varphi) + \varphi F_\varphi(\theta, \varphi). \quad (24)$$

Using the asymptotic representation for Y_{mn} for a p-polarized exciting plane wave the far-field pattern has the form

$$\begin{aligned} F_\theta^p(\theta, \varphi) &= j \sum_{m=0}^M \cos[(m+1)\varphi] (j \sin \theta)^m \sum_{n=1}^{N_c^m} (p_{mn}^e \cos \theta + q_{mn}^e) G_n - j \sin \theta \sum_{n=1}^{N_c^0} r_n^e G_n, \\ F_\varphi^p(\theta, \varphi) &= -j \sum_{m=0}^M \sin[(m+1)\varphi] (j \sin \theta)^m \sum_{n=1}^{N_c^m} (p_{mn}^e + q_{mn}^e \cos \theta) G_n, \\ G_n &= \exp(-jz_n \cos \theta) \end{aligned} \quad (25)$$

The last term in F^p corresponds to vertical dipoles.

For s-polarized excitation the far-field components can be written as follows:

$$\begin{aligned} F_\theta^s(\theta, \varphi) &= j \sum_{m=0}^M \sin(m+1)\varphi (j \sin \theta)^m \sum_{n=1}^{N_c^m} (p_{mn}^e \cos \theta - q_{mn}^e) G_n, \\ F_\varphi^s(\theta, \varphi) &= j \sum_{m=0}^M \cos(m+1)\varphi (j \sin \theta)^m \sum_{n=1}^{N_c^m} (p_{mn}^e - q_{mn}^e \cos \theta) G_n + j \sin \theta \sum_{n=1}^{N_c^0} r_n^e G_n. \end{aligned} \quad (26)$$

4. Numerical results

Next we would like to present some computational results to demonstrate the capabilities of the new concept. An important characteristic of scattering is the differential cross section (DSC):

$$\text{DSC}^{p,s} = |F_\theta^{p,s}(\theta, \varphi)|^2 + |F_\varphi^{p,s}(\theta, \varphi)|^2, \quad (27)$$

where $F_\theta^{p,s}(\theta, \varphi)$ and $F_\varphi^{p,s}(\theta, \varphi)$ are given in equations (25) and (26) respectively. The main parameters of the fibres such as the length and diameter are depicted in figure 2. Firstly we present a comparative result to check the validity of our FORTRAN code based on the approach mentioned above. Initially we verify the results by comparison with those provided by other methods. To this end, we performed computations using the NFM-DS [6]. This method has been developed to compute the \mathbf{T} matrix for elongated scatterers using DSs distributed along the axis of symmetry of a scatterer. Results for prolate spheroids with an aspect ratio of 20 have been published [6]. We have recently extended the



Figure 2. Parameters of one of the fibres.

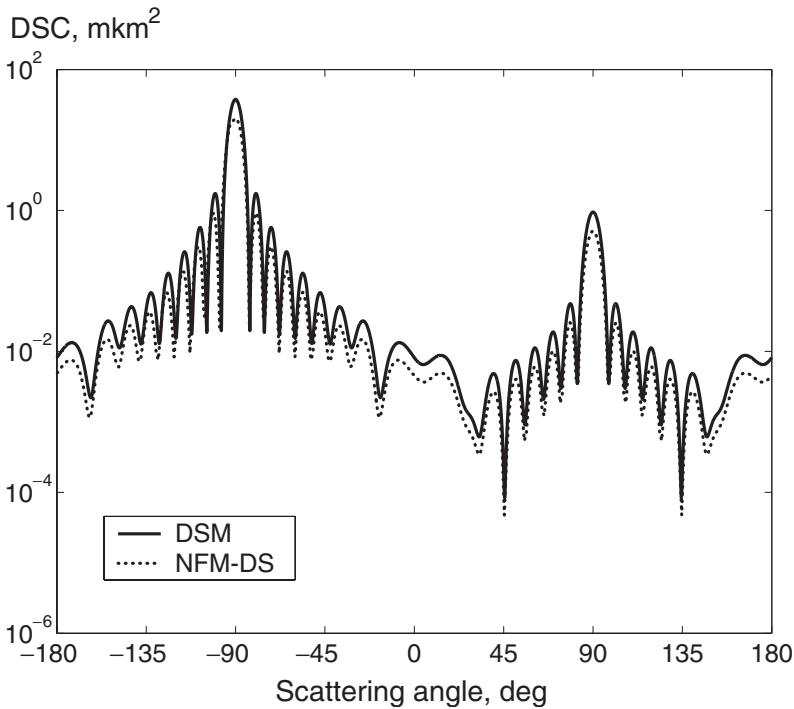


Figure 3. Dependence of p-polarized DSC on the scattering angle θ in the plane of incidence $\varphi = 0$, from a glass ($n = 1.5 - 0.0i$) cylinder, of length $l = 4 \mu\text{m}$, and diameter $D = 0.4 \mu\text{m}$, with an incidence angle θ_0 of the plane wave of 90° and $\lambda = 0.488 \mu\text{m}$: comparison of the two programmes DSM and NFM-DS.

NFM-DS to scattering by cylindrical fibres with rounded ends such that the shape of the cylinder is identical with the particle shape used in the present paper. To be able to validate our new version of the DSM, results computed by both methods are plotted in figures 3 and 4. Here the DSC for a glass ($n = 1.5 - 0.0i$) cylinder having an aspect ratio of 10, a diameter D of $0.4 \mu\text{m}$ and a length of $4 \mu\text{m}$ for p polarization (figure 3) and for s polarization (figure 4) are plotted. In figures 3 and 4, one of the curves (NFM-DS) has been translated in order to allow the reader to distinguish between them. Comparing the data, one can see that there is almost

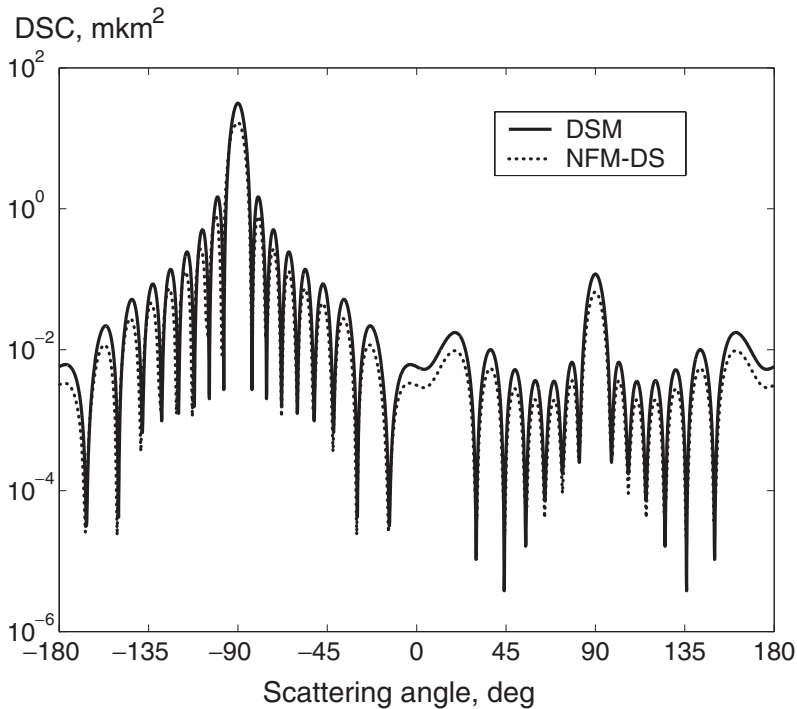


Figure 4. DSC for s polarization from a glass ($n=1.5-0.0i$) cylinder, with $l=4\ \mu\text{m}$, $D=0.4\ \mu\text{m}$, $\theta_0=90^\circ$, and $\lambda=0.488\ \mu\text{m}$: comparison of two programmes.

perfect agreement between the computational results obtained using different codes both for the p- and s-polarized excitation.

To demonstrate the capabilities of the new code we present simulated results corresponding to the largest aspect ratio that we achieved. In figures 5 and 6 the DSC is plotted for a cylinder with an aspect ratio of 100. With this aspect ratio we managed to obtain results for fibres $30\ \mu\text{m}$ long. In figures 7 and 8 we present some results for SiO fibre of the same length with an aspect ratio of 30. Comparing the results for fibres of length $30\ \mu\text{m}$ having different aspect ratios, one can see that the number of oscillations increases with increasing aspect ratio. This effect is well known from the theory of dielectric antenna. It is due to quasisurface waves travelling over the surface of the scatterer.

With the following results we present the largest fibre that we can compute with an aspect ratio of 10. The DSC for SiO fibres with a length of $40\ \mu\text{m}$ and a diameter of $4\ \mu\text{m}$ is plotted in figure 9 (for p-polarized excitation) and figure 10 (for s-polarized excitation).

5. Conclusions

In this paper a renewed scheme of the DSM was applied to analyse light scattering from very elongated fibres. The main differences between the extended DSM scheme and the conventional scheme [8] are as follows: different numbers of DSs are used to represent the scattered field outside and the total field inside the particle; the number of DSs depends on the rank of the Fourier harmonics.

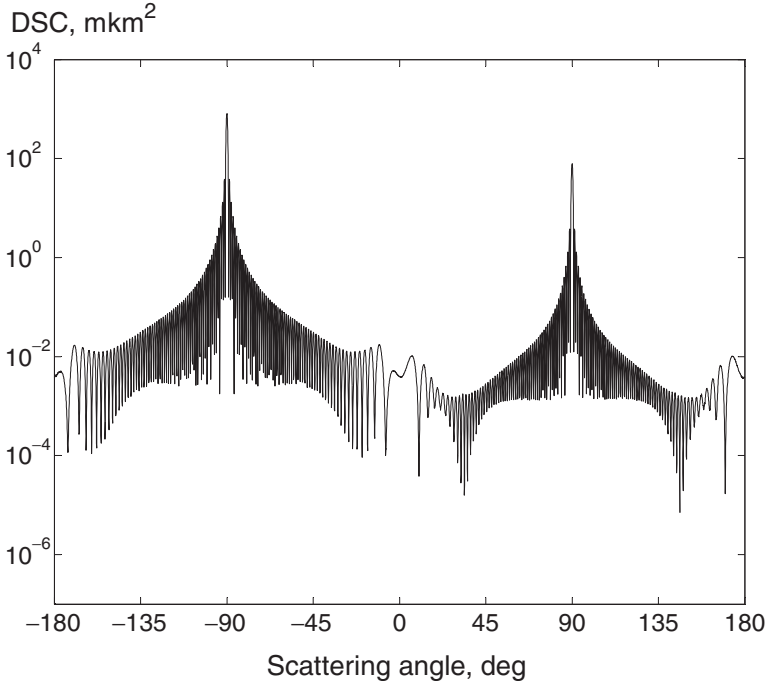


Figure 5. DSC for p polarization from a SiO ($n=1.67 - 0.0i$) cylinder, with $l=30\ \mu\text{m}$, $D=0.3\ \mu\text{m}$, $\theta_0=90^\circ$ and $\lambda=0.488\ \mu\text{m}$.

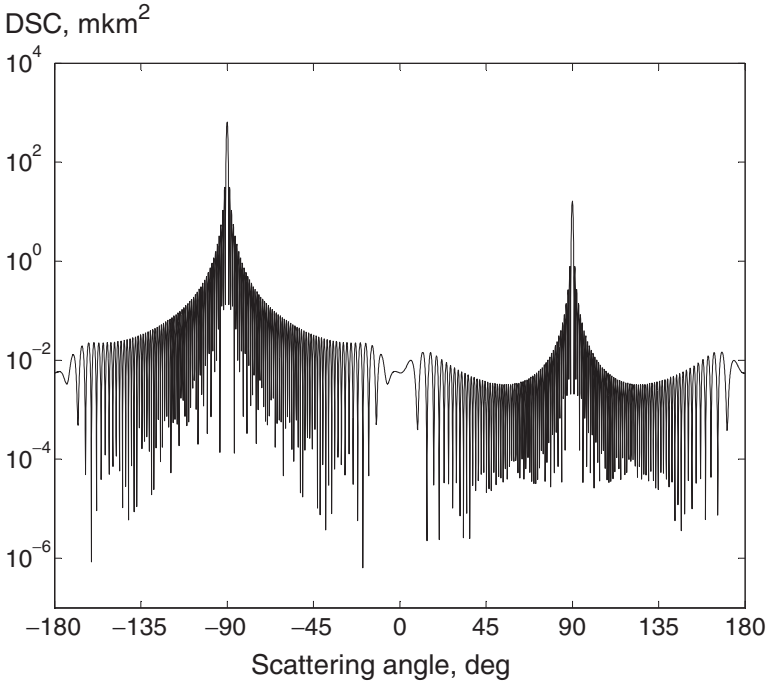


Figure 6. DSC for s polarization from a SiO cylinder, with $l=30\ \mu\text{m}$, $D=0.3\ \mu\text{m}$, $\theta_0=90^\circ$ and $\lambda=0.488\ \mu\text{m}$.

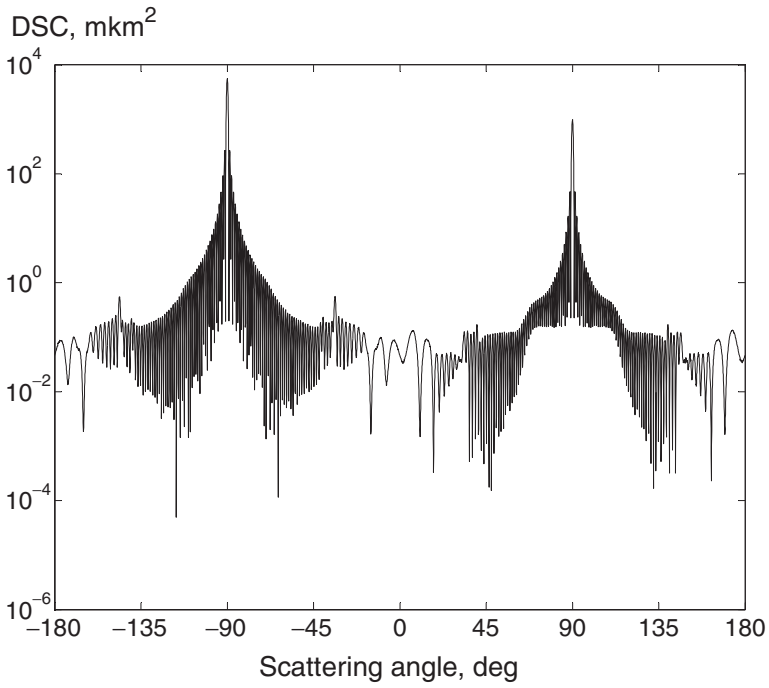


Figure 7. DSC for p polarization from a SiO cylinder with $l = 30 \mu\text{m}$, $D = 1 \mu\text{m}$, $\theta_0 = 90^\circ$ and $\lambda = 0.488 \mu\text{m}$.

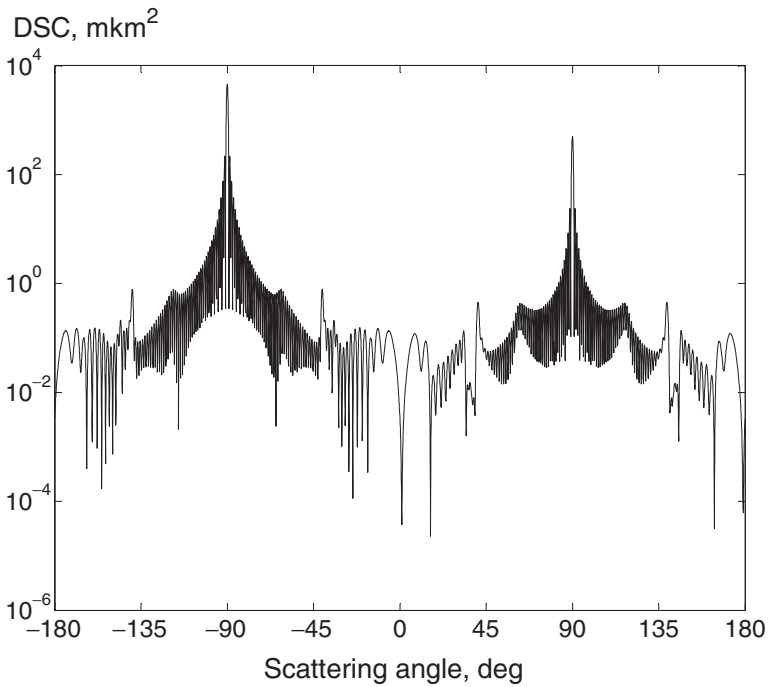


Figure 8. DSC for case of s polarization from a SiO cylinder: $l = 30 \mu\text{m}$, $D = 1 \mu\text{m}$, $\theta_0 = 90^\circ$ and $\lambda = 0.488 \mu\text{m}$.

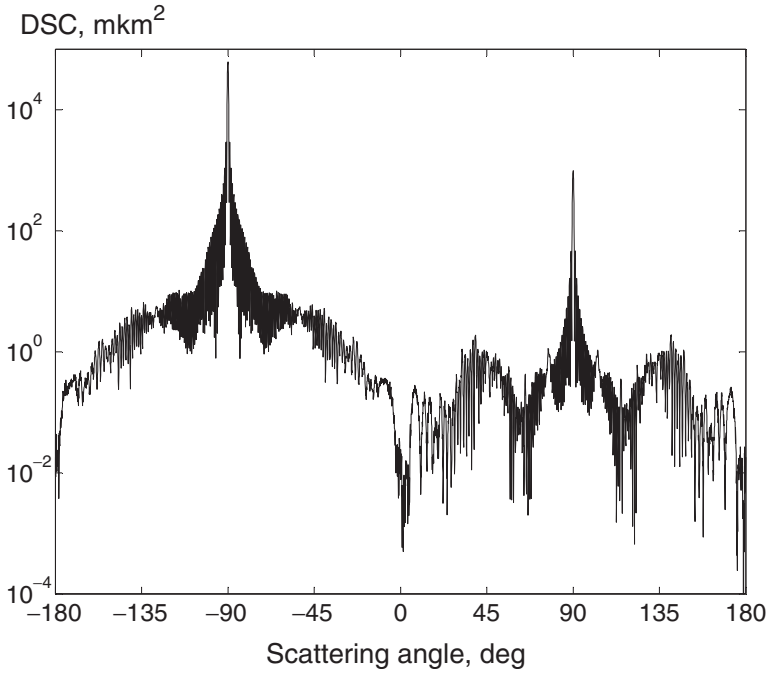


Figure 9. DSC for p polarization from a SiO cylinder with $l=40\ \mu\text{m}$, $D=4\ \mu\text{m}$, $\theta_0=90^\circ$ and $\lambda=0.488\ \mu\text{m}$.

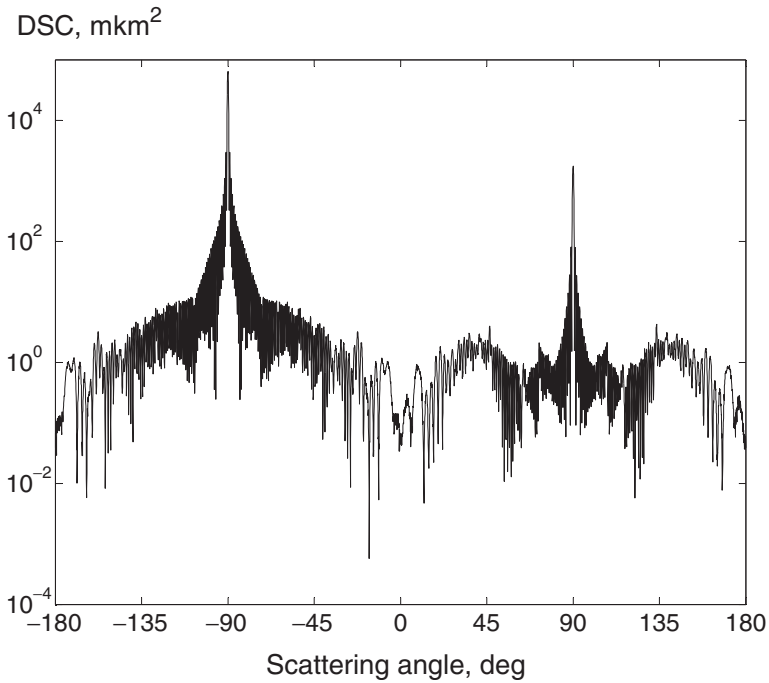


Figure 10. DSC for s polarization from a SiO cylinder with $l=40\ \mu\text{m}$, $D=4\ \mu\text{m}$, $\theta_0=90^\circ$ and $\lambda=0.488\ \mu\text{m}$.

This means that for higher harmonics a lower number of multipoles is used. This enables us to acquire more accurate numerical results, provides a monotonic decrease in the surface residual and reduce computer costs for larger particles compared with the conventional DSM model. Also it allows us to extend the range of validity of the DSM to particles of larger diameters. On the basis of the new approach a FORTRAN code has been developed. This enables us to calculate DSC from fibres with aspect ratios up to 100 and length up to 40 μm .

6. Acknowledgments

We gratefully acknowledge financial support for this research by the Deutsche Forschungsgemeinschaft (DFG) and the Russian Foundation of Basic Research.

References

- [1] FARAFONOV, V., and IL'IN, V., 2001, *Optics Spectrosc.*, **91**, 960.
- [2] WRIEDT, T., 1999, *Generalized Multipole Techniques for Electromagnetic and Light Scattering* (Amsterdam: Elsevier), pp. 5–20.
- [3] AL-RIZZO, H. M., and TRANQUILLA, J. M., 1995, *J. Comput. Phys.*, **119**, 342.
- [4] HAFNER, C., and BOMHOLT, K., 1993, *The 3D electrodynamic Wave Simulator* (Chichester, West Sussex: Wiley).
- [5] SAGEHORN, H., LIST, J., WIEGAND, T., WEICHERT, R., and WRIEDT, T., 2001, *Particle particle Syst. Characteristics*, **18**, 55.
- [6] DOICU, A., and WRIEDT, T., 1997, *Optics Commun.*, **139**, 85.
- [7] EREMIN, Y., and WRIEDT, T., 2002, *Optics Commun.*, **214**, 39.
- [8] EREMIN, Y., ORLOV N., and SVESHNIKOV, A., 1999, *Generalized Multipole Techniques for Electromagnetic and Light Scattering*, edited by T. Wriedt (Amsterdam: Elsevier), pp. 39–80.
- [9] COLTON, D., and KRESS, R., 1992, *Inverse Acoustic and Electromagnetic Scattering Theory* (Berlin: Springer).
- [10] DOICU, A., EREMIN, Y., and WRIEDT, T., 2000, *Acoustic and Electromagnetic Scattering Analysis using Discrete Sources* (San Diego, California: Academic Press).
- [11] VOEVODYN, V., and KUZNETSOV, A., 1982, *Matrices and Calculations* (Moscow: Science) (in Russian).